A View on dust evolution, from Herschel observations of the nearby universe

Frédéric Galliano[*]**, Aurélie Rémy-Ruyer & Suzanne C. Madden**
AIM, Bât. 709, L'Orme des Merisiers, CEA/Saclay, 91191 Gif-sur-Yvette, France
E-mail: frederic.galliano@cea.fr

The observational approach to study dust evolution usually consists of relating measured dust properties to parameters quantifying the physical conditions of a given region. Nearby galaxies constitute, in that sense, unique targets, due to the wide range of heavy element abundances (metallicity) and irradiation conditions they exhibit. Modelling the infrared (IR) to submillimeter (submm) spectral energy distributions (SED) of nearby galaxies observed with *Herschel* & *Spitzer*, nowadays, does not allow us to isolate individual grain processes. However, it is a powerful means to scrutinize the variations of average grain properties with environmental conditions, providing crucial benchmarks for dust evolution models. In particular, the evolution of the dust-to-gas mass ratio with metallicity is one of the keys to understanding cosmic dust evolution. Indeed, individual galaxies, at different metallicities can be considered as snapshots of galaxy evolution, at different stages of their elemental enrichment, despite the possible differences in star formation history.

In this paper, we first summarize a recent study, presenting such a relation, in a sample of 126 nearby galaxies, observed with *Herschel* & *Spitzer* among other telescopes, covering a 2 dex metallicity range. This work shows that the dust-to-gas mass ratio is roughly proportional to the metallicity (Z) above $Z \simeq 1/10 \, Z_\odot$, and becomes non-linear below. Comparing to theoretical evolution models, it indicates that dust condensation in dense clouds is a crucial ingredient, responsible for the change of regime above this critical metallicity. We argue that the scatter in the relation is likely intrinsic, being the consequence of the diversity of star formation histories of each individual galaxy.

Then, we discuss the methodological problems encountered when modelling dust properties and deriving correlations between grain parameters. In particular, we demonstrate that hierarchical Bayesian models can correct the various biases affecting standard least-square SED fits. Although these hierarchical Bayesian models are efficient, they have convergence issues. We demonstrate that these convergence issues can be addressed, using dedicated numerical methods.

[*]Speaker.

1. SED Modelling of a Nearby Galaxy Sample

In order to study the evolution of the dust-to-gas mass ratio (D/G), with an optimal Z coverage, we have merged several nearby galaxy samples: the Dwarf Galaxy Survey (DGS; [9, 12]), the KINGFISH survey [8] and the sample of Galametz [4]. In total, we have 126 sources, ranging from $1/40\,Z_\odot$ to $2.5\,Z_\odot$. For each galaxy, we have collected and processed the following data sets.

- Near-IR-to-submm data (including *Spitzer* and *Herschel*), for estimating the dust mass.

- H I observations, to estimate the atomic gas mass. For galaxies where the H I halo is extended, we integrate the mass encompassed in the aperture used for the IR/submm photometry.

- CO observations, to derive the molecular gas mass. The CO-to-H$_2$ conversion factor (X_{CO}) is very uncertain, especially at low Z. To account for this uncertainty, we consider both the molecular gas masses derived using a Galactic X_{CO}, and using an empirical $X_{CO} \propto Z^{-2}$ [13].

- Strong emission lines, in order to derive a self-consistent metallicity for each object [9].

We fit the global observed SED of each galaxy, using the model of Galliano [6]. This model uses the framework of Galactic grains (PAHs, carbon grains and silicates; [18]), and accounts for the mixing of various starlight intensities in the galaxy. Fig. 1 shows a few SEDs of our sample. Analyzing qualitatively these figures, we notice the following.

- The SED of a quiescent $Z_\odot$ galaxy (NGC 2841) is similar to the Galactic diffuse ISM.

- A $Z_\odot$ starburst (NGC 2146) is on average hotter, the SED peaking at shorter wavelengths. It also has a broader mid-IR-to-submm SED, indicating a large gradient of temperatures, due to the presence of compact star forming regions, mixed with more diffuse ISM.

- At low Z (SBS 1415+437 & II Zw 40), we observe that the total power of the objects is about two orders of magnitude lower (size effect), and that the PAH features are considerably weaker. We also note that the SED is always peaking at shorter wavelengths and broader than the isothermal case (diffuse ISM), independently of the star formation activity.

2. Dust Evolution: Comparing Models to Observations

The SED modelling presented in Sect. 1 allows us to derive a global D/G for each galaxy (Fig. 2). We can see that there is a clear trend of increasing D/G with Z. Moreover, we note that the trend appears steeper than the linear regime (D/G $\propto Z$), although the scatter is significant. The assumed X_{CO}, discussed in Sect. 1, does not qualitatively change the trend. We show here the results solely with the Galactic value. To interpret this observed trend, we have compared it to the dust evolution model of [1] (see also [17]), for different star formation histories (SFH). It accounts for dust formation in stellar photospheres and by condensation in dense clouds, and dust destruction by astration and shocks. The various tracks on Fig. 2 illustrate the following main features.

- At low Z, the grain production is dominated by condensation in stellar ejecta. The trends are roughly linear with Z, but results in dust-to-metal mass ratios (D/Z) two orders of magnitude lower than the Galactic value, due to low stellar dust yields.
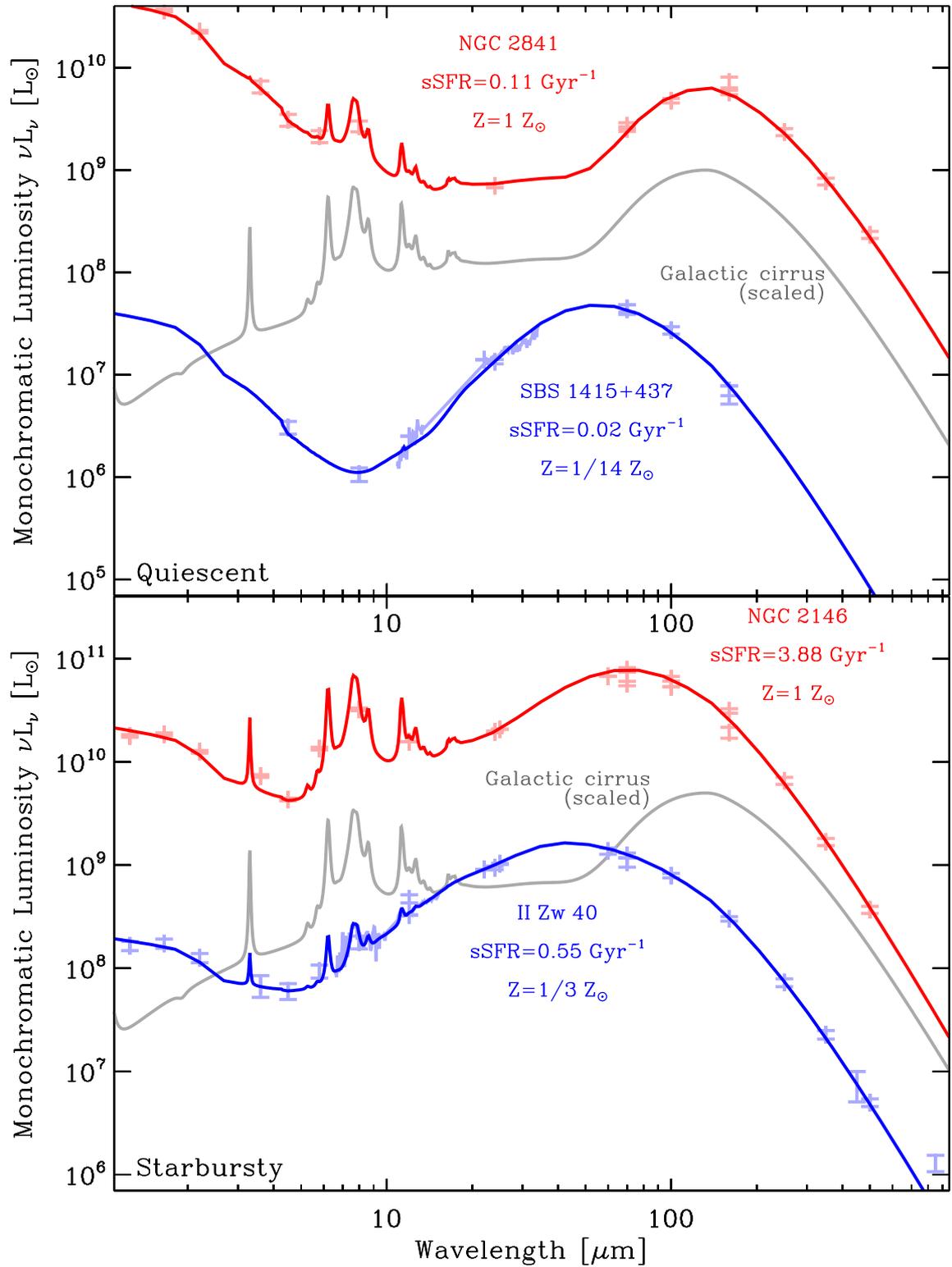
Figure 1: SEDs of select galaxies from our sample [10, 11]. For each galaxy, we overplot the model (solid line) on top of the observed fluxes (error bars). We list the metallicity, as well as the specific star formation rate (sSFR). In each panel, we plot the SED of the diffuse Galactic ISM (no stellar continuum; [18]).
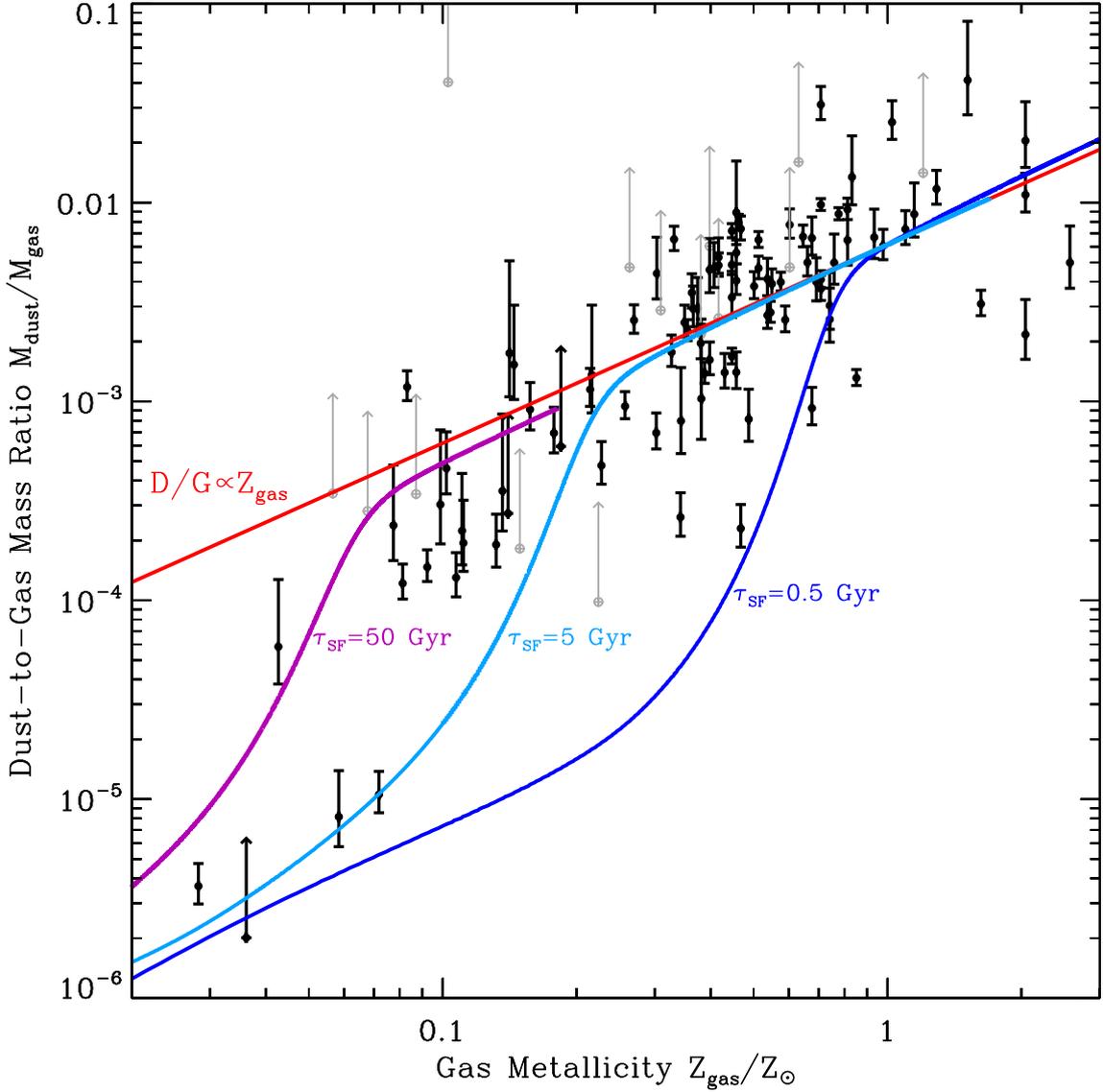
Figure 2: Trend of dust-to-gas mass ratio with metallicity. The points with error bars represent the observed D/G of integrated galaxies, as a function of Z [10]. The color tracks have been obtained with the dust evolution model by [1], with different star formation histories, parametrized by their timescale $\tau_{\rm SF}$.

- Around $Z \simeq 1/10 \, Z_{\odot}$, there is a rapid increase of D/G. Above this *critical metallicity*, dust production becomes dominated by condensation in dense clouds. It is now more efficient, and the D/Z reaches the Galactic value. At this stage, D/G is again linear with Z.

The good agreement between the observed and theroretical D/G suggests that grain condensation in dense clouds is a crucial ingredient to explain the dust content of galaxies. It provides a sound physical argument to support the non-linearity of our trend, explaining the sudden rise of D/G above $Z \simeq 1/10 \, Z_{\odot}$. The scatter in D/G being larger than the uncertainties, we conclude that to perform a more accurate comparison, we would need to account for the proper SFH of each object.

In contrast, several recent studies provide estimates of the dust-to-gas mass ratios of distant
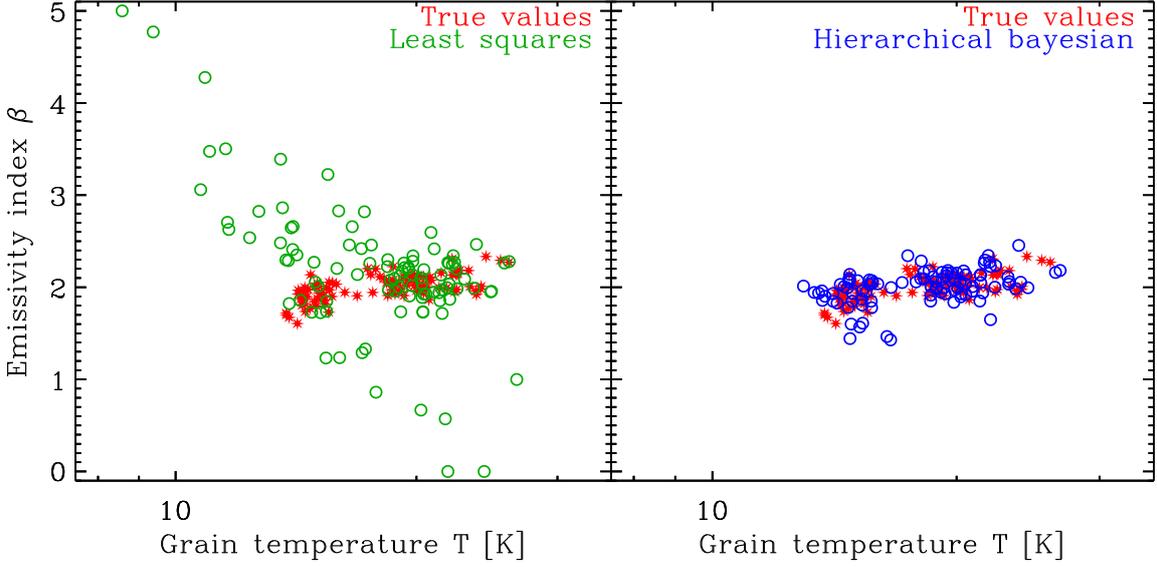
Figure 3: Comparison of χ^2 and hierarchical Bayesian methods. The true values (red) are simulated modified black bodies, with added noise and systematic calibration errors. The resulting simulated SEDs are fit both with a best χ^2 approach (green) and with a hierarchical Bayesian model (blue) [5].

galaxies, measured in extinction, in the UV and X-ray regimes [2, 3, 16]. These studies indicate, somewhat contradictorily, either a constant dust-to-metal mass ratio down to $\simeq 1/100\, Z_\odot$ or a linearly-increasing relation between (primarily Fe-based) dust-to-metal mass ratio and metallicity. Apart from possible methodological biases, these differences with our study could be the result of different star formation histories. In particular, episodic star formation histories can lead to nearly Galactic dust-to-metal mass ratios at very low-metallicity (e.g. [17]).

3. Fine-Tuning the Trends: a Hierarchical Bayesian Approach

Apart from refining the dust evolution modelling, the accuracy of the derived trends might benefit from improving the SED modelling. In particular, the strong non-linearity of dust SED models makes noise and systematic errors a problematic source of biases. The most famous example is the false anti-correlation between grain temperature T and emissivity index β, derived from modified black-body (MBB) fits [14]. Recently, [7] demonstrated that a hierarchical Bayesian (HB) approach could efficiently correct these biases. We have implemented this approach and are currently extending it beyond the simple MBB, to model realistic grain SEDs [5].

The principle of this HB approach is to simultaneously perform a physical modelling (the SED fit) and a statistical modelling of the parameter distribution. Bayes' theorem relates the posterior distribution of the parameters, which is what we are looking for, to the product of their likelihood (derived from SED modelling) and of a *prior* distribution:

$$\underbrace{p(\text{parameters}|\text{observed fluxes})}_{posterior} \propto \underbrace{p(\text{observed fluxes}|\text{parameters})}_{likelihood} \times \underbrace{p(\text{parameters})}_{prior}. \quad (3.1)$$
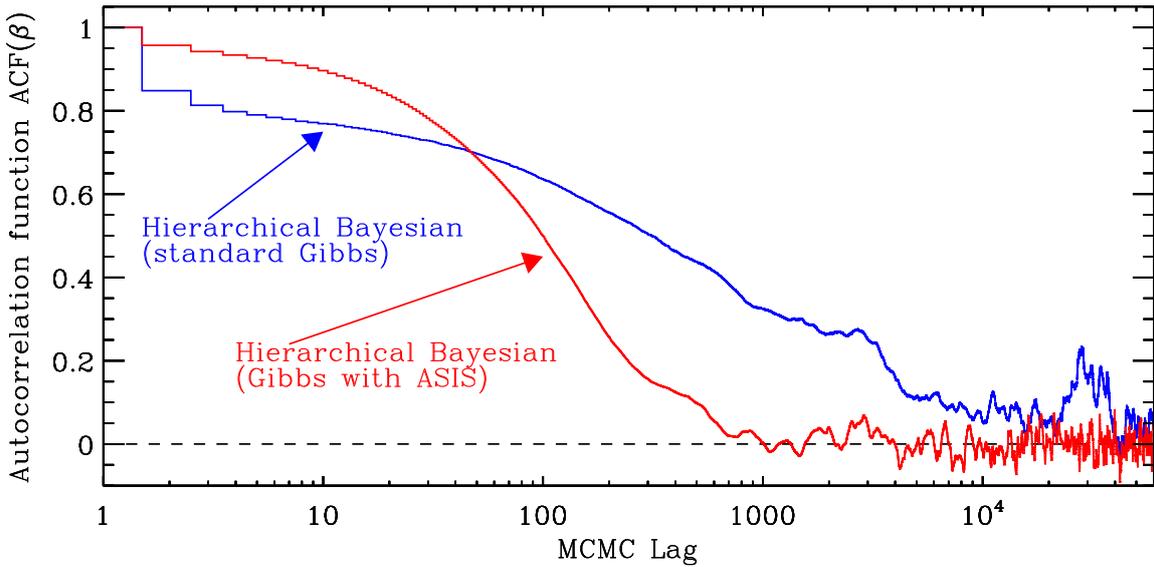
Figure 4: Autocorrelation functions of the mean of β for the MBB simulation. The curves represent the full hierarchical model, using a standard Gibbs sampling (blue), or ASIS (red; [15], also used by [7]) [5].

In a hierarchical model, we solve for the mean and covariance matrix of this prior distribution. In this way, the SEDs having a low signal-to-noise ratio (S/N) are corrected by the statistical knowledge of the distribution of the high S/N sources. This is demonstrated in Fig. 3, using simulated data, for the MBB case. The χ^2 values show the well-known false anticorrelation between T and β, while the HB method is efficient at recovering the statistical properties of our sample.

Usually, HB methods are numerically implemented using Markov Chain Monte Carlo (MCMC). However, these algorithms suffer from convergence issues. Fig. 4 compares the autocorrelation functions (ACF) of several MCMCs. The faster the ACF drops to 0, the more efficient the convergence will be. This figure demonstrates that applying the standard sampling method (Gibbs), to the simple MBB case, will run into convergence issues (even after several 10^5 steps), while applying the method of [15] (ASIS) will ensure convergence with a reasonable MCMC length [7].

References

[1] Asano, R. S., Takeuchi, T. T., Hirashita, H., & Inoue, A. K. 2013, Earth, Planets, and Space, 65, 213

[2] Chen, B., Dai, X., Kochanek, C. S. and Chartas, G., 2013, arXiv:1306.0008

[3] De Cia, A., Ledoux, C., Savaglio, S. Schady, P. and Vreeswijk, P. M., 2013, A&A, 560, A88

[4] Galametz, M., Madden, S. C., Galliano, F., et al. 2011, A&A, 532, A56

[5] Galliano, F. 2014, A&A, *in prep.*

[6] Galliano, F., Hony, S., Bernard, J.-P., et al. 2011, A&A, 536, A88

[7] Kelly, B. C., Shetty, R., Stutz, A. M., et al. 2012, ApJ, 752, 55

[8] Kennicutt, R. C., Calzetti, D., Aniano, G., et al. 2011, PASP, 123, 1347

[9] Madden, S. C., Rémy-Ruyer, A., Galametz, M., et al. 2013, PASP, 125, 600

[10] Rémy-Ruyer, A., Madden, S. C., Galliano, F., et al. 2014, [arXiv:1312.3442]

[11] Rémy-Ruyer, A., Madden, S. C., Galliano, F., et al. 2014, *in prep.*

[12] Rémy-Ruyer, A., Madden, S. C., Galliano, F., et al. 2013, A&A, 557, A95

[13] Schruba, A., Leroy, A. K., Walter, F., et al. 2012, AJ, 143, 138

[14] Shetty, R., Kauffmann, J., Schnee, S., & Goodman, A. A. 2009, ApJ, 696, 676

[15] Yu, Y. & Meng, X.-L. 2011, JCGS, 20, 531

[16] Zafar, T. and Watson, D., 2013, A&A, 560, A26

[17] Zhukovska, S., 2014, A&A, 562, A76

[18] Zubko, V., Dwek, E., & Arendt, R. G. 2004, ApJS, 152, 211